Three-dimensional model of an external gear pump with an experimental evaluation of the flow ripple

Three-dimensional model of an external gear pump with an experimental evaluation of the flow ripple

Alessandro Corvaglia
Politecnico di Torino, Dipartimento Energia, Turin, Italy
alessandro.corvaglia@polito.it

Alessandro Ferrari[1]
Politecnico di Torino, Dipartimento Energia, Torino, Italy
alessandro.ferrari@polito.it

Massimo Rundo
Politecnico di Torino, Dipartimento Energia, Torino, Italy
massimo.rundo@polito.it

Oscar Vento
Politecnico di Torino, Dipartimento Energia, Torino, Italy
oscar.vento@polito.it

KEYWORDS
Fluid power, gear pump, flow meter, fluid dynamics, model, flow rate ripple.

ABSTRACT

A three-dimensional model of an external gear pump and a new application of an algorithm for the measurement of the unsteady flow rate in hydraulic pipes are presented. The experimental delivery flow ripple was compared with the outcomes of a simulation under different operating conditions. A comprehensive computational fluid dynamics model of the pump and of the high-pressure delivery circuit was developed in SimericsMP+®. The pump model considers the clearances, which vary according to the

[1] Corrresponding author. Address: Corso Duca degli Abruzzi 24, 10129, Torino, Italy. Phone: +390110904426

shaft angle, between the tip of the tooth and the inner surface of the stator, as well as between the flanks of the teeth that are in contact. The pump delivery circuit is constituted by a straight pipe with a fixed orifice at the end to generate the load. The model of the entire system was preliminarily validated in terms of delivery pressure ripple. Subsequently, the simulated flow ripple was contrasted with the instantaneous flow rate, measured by means of an innovative flow meter. It was found that the proposed flow meter is reliable in assessing the flow oscillations under the various working conditions.

1. INTRODUCTION

The delivery pressure ripple in positive displacement pumps represents the main source of noise. This ripple is generated by the interaction between flow rate oscillations and the impedance of the circuit [1]. The flow oscillation in turn originates from the volume derivative of the variable chambers, with respect to the rotational angle (kinematic flow ripple), and from the real behavior of the component: non-ideal timing, leakages, compressibility of the fluid and incomplete filling of the variable chambers.

A few studies on the active reduction of the kinematic flow ripple are available in the literature. Edge and Lipscombe [2] developed a multi-lobe cam mechanism to reduce the flow oscillations of an external gear pump. Minav et al. [3] have recently proposed adjusting the angular speed of an axial piston pump by means of a fast torque control of the electric prime mover. A similar method was also implemented by O'Shea [4] on a gerotor pump. The feasibility of inducing high-frequency oscillations of the swash plate in

order to modify chamber volumes was investigated in Kim and Ivantysynova [5] and Casoli et al. [6].

Regardless of the method that is used, its effectiveness has only been assessed so far by measuring the pressure ripple. In fact, although the measurement of such a quantity is a trivial task, the evaluation of the real flow oscillation has always represented a challenge, due to the low dynamics of flow meters.

The most frequently cited procedure for measuring the flow ripple is the ‘‘Secondary Source’’ method [7], which is grounded on an analysis of the pressure wave propagation in a circuit made up of the pump being tested and an auxiliary source of fluid-borne noise. A different technique, based on particle image velocimetry, was used in Garcia-Vilchez et al. [8] and applied to a gerotor pump. However, such methods suffer from some intrinsic limitations and can only be implemented on dedicated test benches.

On one hand, the possibility of measuring the instantaneous flow rate with minimal modifications of the hydraulic circuit is a promising solution that could lead to practical applications, including model validation.

On the other hand, the accuracy of an innovative flow meter can be assessed by means of a reliable simulation model of the pump, since a flow transducer with comparable dynamic characteristics is not available. The pump model should preliminarily be validated on the basis of measurable dynamic quantities, such as the pressure ripple. Different approaches can be used to build a pump model that is able to reproduce delivery pressure oscillations [9]. The simplest approach, as far as lumped parameter models are concerned, involves only three variable control volumes (inlet, delivery, and trapped). In

spite of this simplification, if the main aim of the simulation is to evaluate the delivery pressure ripple, such an approach may be satisfactory, if a very short delivery pipe is installed in order to minimize the amplitude of the oscillations that are due to the unsteady flow field [10]. Otherwise, an approach that allows the pressure waves in the piping system to be simulated is mandatory to analyze the interaction of the pump with the circuit. In this case, a one-dimensional (1D) model of the ducts, considering capacitive, resistive and inertia effects, must be coupled with the pump model. For a more complete analysis of the pump performance, a control volume should be associated with each hydraulic chamber of the pump, so that it is possible to simulate the pressure drop through the port plate and in the meshing region [11–13]. Additional features can be added to the model to study specific aspects, such as cavitation14 or mechanical–hydraulic efficiency [15,16].

The three-dimensional (3D) computational fluid dynamics (CFD) simulation represents the best methodology to obtain detailed knowledge of the pressure field inside the pump. Nowadays, with the increase in computational capabilities, the 3D simulation of an entire circuit is becoming more and more feasible. External gear pump models have been developed in OpenFOAM® [17, 18], in ANSYS Fluent® [19] and in ANSYS CFX® [20].

A specific template that can be used to manage the mesh in gear pumps is available in SimericsMP+®, which was formerly known as PumpLinx [21]. The code has been proved to be very reliable for the simulation of all types of gear machines, namely internal gears [22], gerotors [23] and external gear pumps [24]. The latter machine type is the most common pump used in constant displacement hydraulic power units, but it features very

high flow oscillations. The possibility of directly measuring such a ripple could be useful to determine the source of the fluid-borne noise that generates air-borne noise [25].

In this framework, the aim of this study is the application of a high-dynamics flow meter (the commercial name is Flotec), developed for unsteady flow rates in high-pressure pipelines, which was successfully tested on a proportional high-performance hydraulic valve [26] and on diesel injection systems [27, 28], to measure the flow ripple of a fluid power gear pump.

2. COMPONENT DESCRIPTION

The reference pump used for this study is a Casappa Magnum HDP 30.51 external gear unit, which is shown in Figure 1, with displacement 51.5 cc/rev, a maximum working pressure of 230 bar and speed in the 300–2500 r/min range. The casing houses a couple of rotors with 10 teeth integral to the shafts and the journal bearings are mounted directly in the two covers. The gears have an external diameter of 57 mm and an axial width of 33 mm.

The balance plates (also referred to as port plates), used to compensate for the axial clearances (cf. Figure 2), are provided with millings in order to manage the connections of the fluid with either the delivery or the suction environment during the compression phase. The clamping force exerted by the balance plates depends on the surface of influence at the rear of the port plates, where the delivery pressure acts. Seals are used to separate the high- from the low-pressure regions. Fluctuations of the pressure force on the gears and leakage flow oscillations, which can both be due to changes in the

clearance between tooth tip and stator (these changes are caused by variations in the loading conditions, the speed or the fluid temperature), are minimized because the oil can flow from the delivery volume to the tooth spaces, through the backflow grooves and the peripheral channels in the balance plates.

3. TEST RIG AND INNOVATIVE FLOW METER

The pump was tested on a hydraulic rig installed at the Fluid Power Research Laboratory of the Politecnico di Torino. The pump was mounted in a closed circuit and driven by a variable-speed electric motor.

The Flotec flow meter was installed at the delivery port. It includes two GS XPM5 miniaturized pressure transducers, which are indicated as P1 and P2 in Figure 3.

The transducers are temperature-compensated between 0 C and 60 C, with a 0–200 bar measuring range, a sensitivity of 100 mV F.S. and linearity error lower than ±0.25% F.S. The GS XPM5 sensing element consists of a (temperature-compensated) Wheatstone bridge, which includes strain gauges. The zero offset of the transducers has been adjusted in order to obtain a measure of 0 bar when the system is not in pressure. It has been assumed that only the transducers accuracy affects the uncertainty, hence the latter is lower than 0.5 bar (according to the linearity error).

The two pressure transducers are installed, at a distance of L = 450 mm, on a straight steel pipe with an internal diameter d = 10 mm. The holes for the transducers were drilled on steel cylinders previously machined and welded on the pipe.

The value of the aspect-ratio L/d = 45 is high enough to avoid errors in the measurement of the instantaneous flow rate [27]. Furthermore, an optimal value of L should be

significantly higher than $2a\Delta t$ [28]. These constraints could lead to a not negligible total length of the straight pipe in case of high displacement pumps due to the high size of the delivery port that induces a subsequent increase in the value of *d*; however, such a length would not represent a limitation for a laboratory instrumentation.

The flowmeter algorithm is based on continuity and momentum balance partial differential equations, written for a one-dimensional flow. Based on the incompressible flow hypothesis and on the continuity equation, the momentum balance equation can be simplified as follows:

$$\frac{\partial u}{\partial t} + \frac{1}{\rho}\frac{\partial p}{\partial x} = -\frac{4\tau_w}{\rho d} \qquad (1)$$

where u is the flow velocity, p is the pressure, ρ is the fluid density and τ_w is the wall shear stress. Multiplying Eq. 1 by the pipe cross-section area A , then integrating the thus achieved equation over length *L* (the distance between the transducers) and finally dividing it by the same *L,* one obtains:

$$\frac{d\bar{Q}}{dt} = \frac{A}{\rho L}\Delta p - \pi d\,\frac{\langle \bar{f} \rangle}{8A^2}\langle \bar{Q} \rangle |\langle \bar{Q} \rangle| \qquad (2)$$

where $\bar{Q}$ represents the space averaged volumetric flow rate, Δp is the instantaneous pressure difference measured by means of the pressure transducers and $\bar{f}$ is the space averaged friction factor (the wall shear stress has been developed by using the Darcy-Weisbach approach). Quantities between angular brackets (< >) are time-averaged. The instantaneous pressure difference can be expressed as a Fourier series [28]:

$$\Delta p(t) \approx \langle \Delta p \rangle + \sum_{k=1}^{N} \left[a_k \cos(\omega_k t) + b_k \sin(\omega_k t)\right] \qquad (3)$$

where a_k and b_k (with $k \geq 1$) are the coefficients of the k-th harmonic term, which refers to angular frequency $\omega_k = 2k\pi / T$, and N is the maximum wave-number that includes 95% of the energy of the Δp Fourier spectrum. Eq. 2 can be integrated over a complete working cycle and, under the hypothesis of periodic flow, one obtains [27]:

$$\frac{A}{\rho L}\langle \Delta p \rangle = \pi d \frac{\langle \bar{f} \rangle}{8A^2} \langle \bar{Q} \rangle |\langle \bar{Q} \rangle| \tag{4}$$

The flow rate fluctuations around the mean value are then obtained through the following equation, which is achieved by substituting Eq. 3 into Eq. 2 and by taking Eq. 4 into account [27, 28]:

$$\Delta Q(t) = \frac{A}{\rho L} \sum_{k=1}^{N} \left\{ \frac{a_k}{\omega_k} \sin\left(\omega_k t\right) - \frac{b_k}{\omega_k} \cos\left(\omega_k t\right) \right\} \tag{5}$$

The instantaneous flow-rate can be finally estimated as $\bar{Q}(t) = \langle \bar{Q} \rangle + \Delta \bar{Q}(t)$.

Time-averaged flow rate $\langle \bar{Q} \rangle$ can be evaluated on the basis of the pump displacement V, the pump speed ω and its volumetric efficiency η_v or can be measured by means of a steady-state low-pressure flowmeter applied to the circuit where the pump is installed. In fact, Eq. (4) is critical for the evaluation of the mean flow-rate, due to the zero-offset errors of the pressure transducers.

Proportional closed-loop controlled valves can be used to choose the inlet and outlet pressures of the pump. However, in order to have a simple layout that is suitable for the validation of the pressure ripple, the load was generated by means of a calibrated orifice with a diameter of 4 mm, drilled into a plate clamped between two flanges and located

at the outlet of the high-pressure flow meter (downstream of transducer P_2). A section view of the delivery line, with details of the two ends, is shown in Figure 4.

A GS XPM5 pressure transducer, with 0–20 bar measuring range, was mounted directly onto the pump casing in order to monitor the pressure in the inlet volume. The excitation voltage (10 Vdc) sent to all pressure transducers was supplied by an Entran MSC-A1 conditioning module, with a frequency band of 0–50 kHz at -1 dB. The same unit was used to amplify the output signals, which were acquired with a sampling frequency of 50 kHz, through a 16 bit NI 6250 National Instruments data acquisition card, with a multi-channel sampling rate of 1 MS/s. The gain in the entire measuring chain, in terms of bar/V, was checked using a deadweight tester. An ISO VG46 Mobil DTE 25 hydraulic oil was used as the fluid in the circuit. The tests were performed at an oil temperature of about 30 °C.

4. CFD MODEL

The pump and delivery pipe model was developed in SimericsMP+ v5.0, where the governing equations were discretized by means of a finite volume method. The surfaces of the fluid domain were extracted, in standard triangulation language (STL) format, starting from the 3D computer-aided design (CAD) model of the pump. The gear profiles were generated analytically, starting from the geometric parameters, and the 3D drawings were then created by extruding the profiles. A 3D view of the pump model is shown in Figure 5.

Since direct contact between the gears is not possible in the model, a minimum distance between the flanks of the teeth of 16 lm was used in the meshing region. Such a clearance was obtained by means of an initial rotation of the driver gear by 0.28°.

Due to the resolution with which the profiles of the gears were imported, it was found that the clearance of 16 μm is the minimum value that allows avoiding interference between the flanks of the gears for any angular position.

In this kind of machines, a critical aspect is represented by the tooth tip clearance that is function of the current eccentricity between the shafts and the bearings. Therefore, compatibly with the fact that in the model the axes are fixed, an operating condition as much realistic as possible was assumed. Hence, for simulating the effect of the radial force acting on the gears, their axes were shifted so that the diametrical clearance was shared 10% at the inlet side and 90% at the outlet side. In this way, a linear increment of the tooth tip clearance is obtained as the chamber moves from the suction to the delivery volume.

The axial clearance between the gears and the port plates was neglected. This assumption is reasonable, since the clearances are mainly compensated for by the micro-movement of the balance plates.

The rotating mesh was generated with a specific template for external gear pumps, which allows a structured hexahedral grid to be obtained for each gear. The number of cells in the radial direction is maintained constant during the rotation and the grid is compressed in the meshing region when a tooth of the opposite gear enters the tooth space. The cell nodes that are in contact with a gear profile are anchored to the latter, while the outermost layer of the cells is made to slide with respect to the casing and to the mesh of the opposite gear. The cells were also squeezed in correspondence to the teeth clearance. A total of 720 cells were set in the circumferential direction and 10 cells in the radial

direction. Details of the grid in the meshing region and in the tooth tip clearance region are visible in Figure 6.

The remaining fluid volumes were meshed with a general mesh generator that allows an unstructured Cartesian grid to be obtained with cubic elements. Four different regions were defined: the inlet volume, the delivery volume, the straight delivery pipe, and the volumes of the grooves on the port plate; the latter were meshed with a finer grid. Moreover, the cells lying on the boundary of each volume feature a higher density. A mesh sensitivity analysis was then carried out, and it was found that the number of cells mainly influences the mean value of the delivery pressure. The delivery pressure oscillation, in correspondence to pressure transducer P1, is plotted in Figure 7 for three values of the total number of cells. A variation in the number of cells in the 462.000–1.8 million range has a negligible effect on the pressure waveform, even though an appreciable effect has been observed for the simulated pressure signal phase. Moreover, it has been verified that 1.5 million cells are adequate to obtain mesh independent results, in terms of an instantaneous pump-delivered flow rate. Since the computational efforts increase significantly when the number of cells becomes very large, the configuration with 1.5 million cells was selected. The corresponding typical grid sizes of the different regions are reported in Table 1.

As far as the physical models are concerned, the flow module is used to solve the mass and momentum conservation equations. The integral form of Reynold's Averaged Navier-Stokes Equations (RANS) is defined as follows:

$$\frac{\partial}{\partial t}\int_{\Omega(t)} \rho d\Omega + \int_{\sigma} \rho\left(\mathbf{v}-\mathbf{v}_{\sigma}\right)\cdot\mathbf{n}d\sigma = 0 \tag{1}$$

$$\frac{\partial}{\partial t}\int_{\Omega(t)} \rho\mathbf{v}d\Omega + \int_{\sigma} \rho\left(\mathbf{v}-\mathbf{v}_{\sigma}\right)\cdot\mathbf{n}\cdot\mathbf{v}d\sigma = \int_{\sigma}\left[\boldsymbol{\tau}\right]\cdot\mathbf{n}d\sigma - \int_{\sigma} p\mathbf{n}d\sigma + \int_{\Omega}\mathbf{f}d\Omega \tag{2}$$

where **v** is the fluid velocity, σ is the control surface, **n** is the outward normal of surface σ, $\mathbf{v}_{\sigma}$ is the velocity of surface σ, ρ is the fluid density, p is the pressure, **f** is the vector of the source terms and $[\boldsymbol{\tau}]$ is the shear tensor stress. The components of the shear stress tensor are:

$$\tau_{ij} = (\mu + \mu_T)\left(\frac{\partial u_i}{\partial x_j} + \frac{\partial u_j}{\partial x_i} - \frac{2}{3}\frac{\partial u_k}{\partial x_k}\delta_{ij}\right) \tag{3}$$

where u_i (i = 1,2,3) are the velocity components, μ is the dynamical viscosity of the fluid, μ_T is the turbulent viscosity and δ_{ij} is the Kronecker Delta function.

The conjugate gradient squared (CGS) linear solver was used for the velocity, while the algebraic multigrid (AMG) solver was applied for the pressure. The turbulence model was deactivated ($\mu_T = 0$), since it was demonstrated, in previous studies, that its effect was negligible [29].

The pressure was set, as a boundary condition, at the inlet port and downstream from the fixed orifice that simulates the load. The conjugate gradient squared linear solver was used for the velocity, while the algebraic multi-grid solver was applied for the pressure. Pressure–velocity coupling was performed with the SIMPLE-S algorithm. The cavitation module was enabled, even though, for the aims of this study, it had no influence on the pressure at the pump delivery port.

5. RESULTS

The model of the pump with the delivery line up to the fixed orifice has been validated in terms of pressure ripple. The simulations were performed, with an angular step of 0.5°, on a workstation with an eight-core Xeon processor at 3.4 GHz. The time required to simulate a complete revolution of the shaft is about 12 h; 2–3 revolutions are usually required to obtain a steady-state point.

The delivery pressure, measured by means of transducer P1, is plotted, as a function of the shaft angle, under three different operating conditions: at 1000 r/min and 45 bar in Figure 8, at 1500 r/min and 95 bar in Figure 9, and at 1750 r/min and 133 bar in Figure 10.

A low-frequency oscillation of the mean value of the delivery pressure was observed at 1750 r/min. Such behavior was also reproduced by the model and was ascribed to the interaction between the pump and the delivery circuit.

Once the model had been validated experimentally, in terms of pressure, the outcomes from the simulation were used to assess the reliability of the flow oscillation measurements and for a further validation of the model.

Figures 11 to 13 show the results of a comparison between the flow rate calculated by the CFD model and the flow rate measured by means of the Flotec flow meter. The curves have been superimposed in order to obtain the same mean flow rate calculated by the CFD model (Flotec does not measure an absolute flow rate but rather the fluctuation with respect to an average value). For the reported results, the Flotec uncertainty can be considered lower than 0.26 l/min [27].

A very satisfactory agreement has been obtained in terms of flow oscillations, in all the analysed configurations (for the sake of conciseness, only three working points are reported). Therefore, the Flotec approach has been found to give accurate flow rate results, and the dynamical model of the pump has also been further validated by the results of the comparison. Moreover, the model for the fluid leakages through the pump, which can have a significant impact on high-pressure systems [30], and particularly on the prediction of the instantaneous flow rate, has been shown to be adequate.

6. CONCLUSIONS

The CFD model of a fluid power external gear pump, developed in SimericsMP+, has been presented. The 3D computational domain considered in the model includes all the internal volumes between the suction port of the pump and the fixed orifice that generates a counterpressure at the end of the high-pressure delivery duct. The simulation of the complete piping system, located downstream from the pump, was necessary to accurately validate the dynamic behavior of the pump. However, the high-pressure test circuit, installed at the pump delivery, was deliberately simplified in order to reduce the computation efforts. Furthermore, thick wall steel ducts were used in the experimental system to avoid the uncertainty that could occur because of the deformation of the pipe walls. A comparison between the simulated and experimental pressure amplitudes at the pump delivery has shown a very satisfactory agreement, without any specific tuning of the model.

The model, validated in terms of pressure, was then applied to assess the accuracy of the Flotec device, which supplies the real flow ripple of the pump. The excellent agreement

that was achieved between the Flotec and the model flow rate oscillations, under all three analyzed operating conditions, has demonstrated that the Flotec principle, already validated in other applications, can also be used for gear pumps installed in fluid power systems.

Furthermore, the here presented results can also represent a further validation of the developed pump model in terms of instantaneous delivered flow rate.

NOMENCLATURE

A	cross-section of the pipe
a	fluid speed of sound
a_k, b_k	coefficients of the k-th harmonic term of the Δp Fourier series
d	internal diameter of the delivery-pipe
$\mathbf{f}$	body force (source term) vector
f	friction factor
L	distance between the transducers
$\mathbf{n}$	outward normal-to-control volume surface
N	total number of harmonics in the Fourier series of Δp
p	pressure
Q	volumetric flow-rate
$\bar{Q}$	average volumetric flow-rate
δ_{ij}	Kronecker delta function
Δp	instantaneous pressure difference
ΔQ	instantaneous flow-rate fluctuations with respect to the mean value
Δt	measurement time step
V	pump displacement
$\mathbf{v}$	fluid velocity vector
$\mathbf{v}_\sigma$	surface velocity vector
ρ	fluid density

μ	fluid dynamical viscosity
σ	control volume surface
$[\boldsymbol{\tau}]$	shear stress tensor
τ_w	wall shear stress
ω	shaft angular speed
ω_k	circular frequency
Ω	control volume

7. REFERENCES

1. Catania, A. E., Ferrari, A., and Mittica, A., 2006, "A High-Pressure Rotary Pump Performance in Multijet Common Rail Systems", Proceedings of the 8th Biennal ASME conference on Engineering System Design and Analysis, Vol. 4: Fatigue and Fracture, Heat Transfer, Internal Combustion Engines, Manufacturing, and Technology and Society: 557-565, ESDA2006-95590.
2. Edge, K.A., Lipscombe, B.R., 1987, "The reduction of gear pump pressure ripple", Proc. IMechE 201:99-106. DOI: 10.1243/PIME_PROC_1987_201_052_02.
3. Minav, T.A., Laurila, L.I.E., Pyrhönen, J.J., 2011, " Axial Piston Pump Flow Ripple; Compensation by Adjusting the Pump Speed with an Electric Drive", The 12th Scandinavian International Conference on Fluid Power, May 18-20, 2011, Tampere, Finland.
4. O'Shea, C., 2016, "Hydraulic Flow Ripple Cancellation Using the Primary Flow Source", BATH/ASME Symposium on Fluid Power and Motion Control, September 7-9, 2016, Bath, UK.
5. Kim, T., Ivantysynova, M., 2017, "Active Vibration/Noise Control of Axial Piston Machine Using Swash Plate Control". Proceedings of the ASME/BATH 2017 Symposium on Fluid Power and Motion Control, Sarasota, USA, 16–19 October 2017.
6. Casoli, P., Pastori, M., Scolari, F., Rundo, M., 2019, "Active Pressure Ripple Control in Axial Piston Pumps through High-Frequency Swash Plate Oscillations—A Theoretical Analysis", Energies 12, 1377. DOI: 10.3390/en12071377.
7. Edge, K.A., Johnston, D.N., 1990, "The 'Secondary Source' Method for the Measurement of Pump Pressure Ripple Characteristics Part 1: Description of Method" Proc. IMechE Part. A: Journal of Power and Energy 204(1): 33-40. DOI: 10.1243/PIME_PROC_1990_204_006_02.
8. Garcia-Vilchez, M., Gamez-Montero, P.J., Codina, E., Castilla, R., Raush, G., Freire, J., Rìo, C., 2015, "Computational fluid dynamics and particle image velocimetry assisted design tools for a new generation of trochoidal gear pumps", Advances in Mechanical Engineering 7(7): 1-14. DOI: 10.1177/1687814015592561.
9. Rundo, M., 2017, "Models for Flow Rate Simulation in Gear Pumps: A Review", Energies 10(9), 1261, 2017. DOI:10.3390/en10091261.

10. Mancò, S., Nervegna N., 1989, “Simulation of an external gear pump and experimental verification”, 1st JHPS International Symposium on Fluid Power, Tokyo, Japan, Mar. 13-16, 1989.
11. Eaton, M., Keogh, P.S., Edge, K.A., 2006, “The modelling, prediction, and experimental evaluation of gear pump meshing pressures with particular reference to aero-engine fuel pumps”, Proc. IMechE Part I 220(5): 365-379. DOI: 10.1243/09596518JSCE183.
12. Vacca, A., Franzoni, G., Casoli, P., 2007, “On the analysis of experimental data for external gear machines and their comparison with simulation results”. ASME International Mechanical Engineering Congress and Exposition, Seattle, USA, 11–15 November 2007. DOI: 10.1115/IMECE2007-42664.
13. Wang, S., Sakura, H., Kasarekar, A., 2011, “Numerical modelling and analysis of external gear pumps by applying generalized control volumes”, Mathematical and Computer Modelling of Dynamical Systems, 17(5): 501-513. DOI: 10.1080/13873954.2011.577556.
14. Zhou, J., Vacca, A., Casoli, P., 2014, “A novel approach for predicting the operation of external gear pumps under cavitating conditions”, Simul. Model. Pract. Theory, 45: 35-49. DOI: 10.1016/j.simpat.2014.03.009.
15. Borghi, M., Zardin, B., 2015, “Axial Balance of External Gear Pumps and Motors: Modelling and Discussing the Influence of Elastohydrodynamic Lubrication in the Axial Gap”, ASME International Mechanical Engineering Congress and Exposition, Houston, USA, Nov 13-19 2015. DOI:10.1115/IMECE2015-51632.
16. Zardin, B., Natali, E., Borghi, M., 2019, “Evaluation of the hydro - Mechanical efficiency of external gear pumps”, Energies 12(13), 2468. DOI: 10.3390/en12132468.
17. Del Campo, D., Castilla, R., Raush, G.A., Gamez Montero, P.J., Codina, E., 2012, “Numerical analysis of external gear pumps including cavitation”, J. Fluids Eng. 134(8), 081105. DOI: 10.1115/1.4007106.
18. Castilla, R., Gamez-Montero, P.J., Del Campo, D., Raush, G., Garcia-Vilchez, M., Codina, E., 2015, “Three-dimensional numerical simulation of an external gear pump with decompression slot and meshing contact point”, J. Fluids Eng. 137(4), 041105. DOI: 10.1115/1.4029223.
19. Strasser, W., 2007, “CFD investigation of gear pump mixing using deforming/agglomerating mesh”, J. Fluids Eng. 129(4): 476-484. DOI: 10.1115/1.2436577.
20. Yoon, Y., Park, B.H., Shim, J., Han, Y.O., Hong, B.J., Yun, S.H., 2017, “Numerical simulation of three-dimensional external gear pump using immersed solid method”, Applied Thermal Engineering 118:539-550. DOI: 10.1016/j.applthermaleng.2017.03.014.
21. Ding, H., Visser, F.C., Jiang, Y., Furmanczyk, M., 2011, “Demonstration and validation of a 3D CFD simulation tool predicting pump performance and cavitation for industrial applications”, J. Fluids Eng. 133(1):011101. DOI: 10.1115/1.4003196.

22. Jiang, Y., Furmanczyk, M., Lowry, S., Zhang, D. et al., "A Three-Dimensional Design Tool for Crescent Oil Pumps", SAE Technical Paper 2008-01-0003, 2008. DOI: 10.4271/2008-01-0003.
23. Altare, G., Rundo, M., 2016, "Computational Fluid Dynamics Analysis of Gerotor Lubricating Pumps at High-Speed: Geometric Features Influencing the Filling Capability", J. Fluids Eng. 138(11), 111101. DOI: 10.1115/1.4033675.
24. Frosina, E., Senatore, A., Rigosi, M., 2017, "Study of a high-pressure external gear pump with a computational fluid dynamic modeling approach", Energies 10(8), 1113. DOI: 10.3390/en10081113.
25. Woo, S., Opperwall, T., Vacca, A., Rigosi, M., 2017, "Modeling noise sources and propagation in external gear pumps", Energies 10(7), 1068. DOI: 10.3390/en10071068
26. Ferrari, A., Pizzo, P., Rundo M., 2018, "Modelling and experimental studies on a proportional valve using an innovative dynamic flow-rate measurement in fluid power systems", Proc. IMechE Part C: J. Mechanical Engineering Science 232(13): 2404-2418. DOI: 10.1177/0954406217721259.
27. Ferrari, A., Pizzo, P., 2016, "Optimization of an Algorithm for the Measurement of Unsteady Flow-Rates in High-Pressure Pipelines and Application of a Newly Designed Flowmeter to Volumetric Pump Analysis", J. Eng. Gas Turbines Power, 138(3): 031604. DOI:10.1115/1.4031541.
28. Catania, A. E., Ferrari, A., 2009, "Development and Assessment of a New Operating Principle for the Measurement of Unsteady Flow Rates in High Pressure Pipelines" in Flow Meas. Instrum., 20(6): 230-240. DOI: 10.1016/j.flowmeasinst.2009.08.004.
29. Rundo, M., Altare, G., 2018, "Lumped Parameter and Three-Dimensional Computational Fluid Dynamics Simulation of a Variable Displacement Vane Pump for Engine Lubrication", J. Fluids Eng. 140(6): 061101. DOI: 10.1115/1.4038761.
30. Ferrari, A., Mittica, A., Pizzo, P., Wu, X., and Zhou, H., 2018, "New Methodology for the Identification of the Leakage Paths and Guidelines for the Design of Common Rail Injectors with Reduced Leakages", ASME Journal of Engineering for Gas Turbines and Power , 140(2), p 022801 (10 pages).

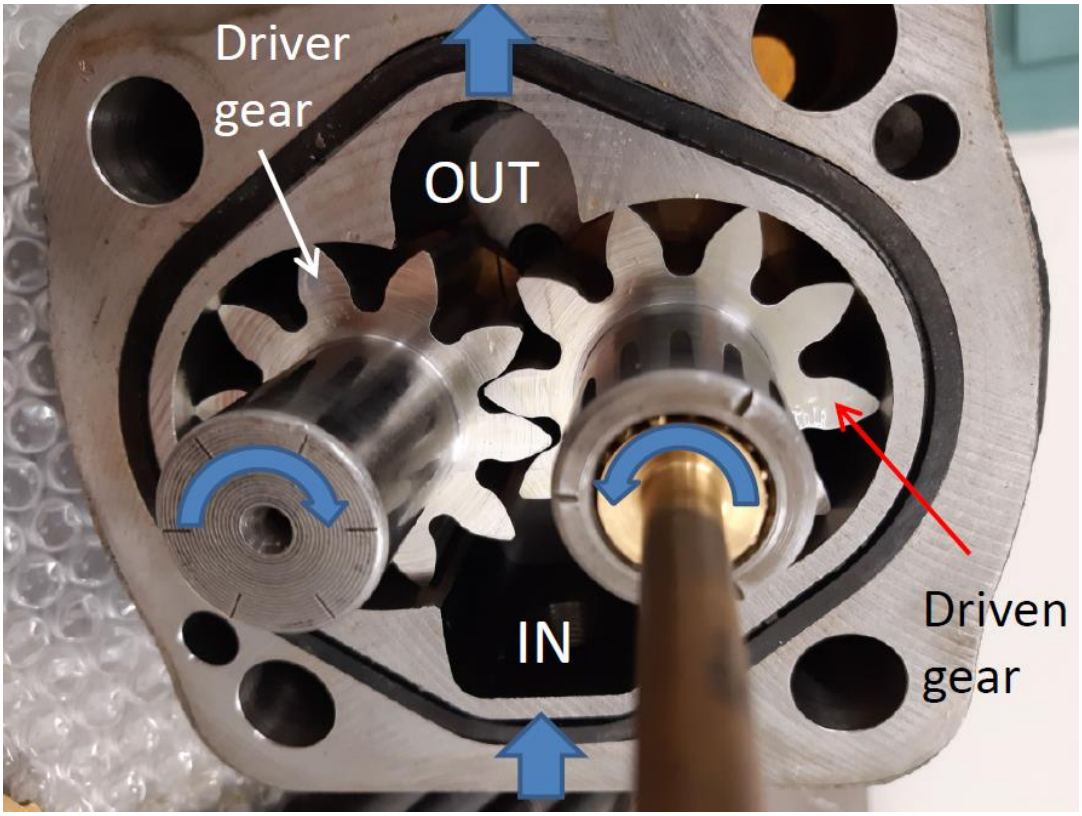

Figure 1: view of the external gear pump

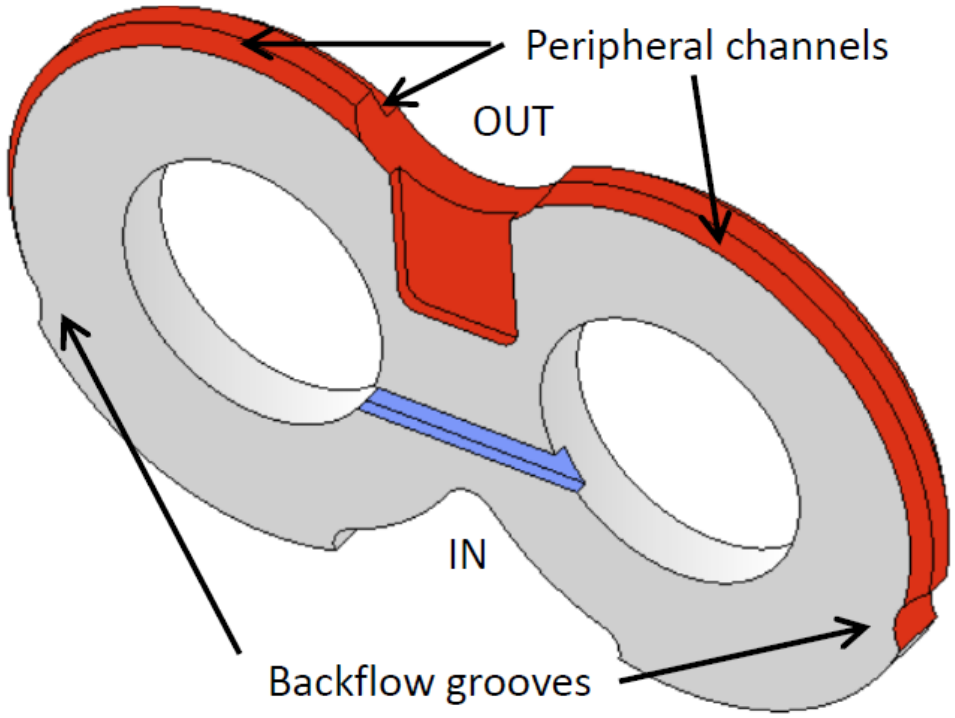

Figure 2: 3D drawing of a balance plate (gear side)

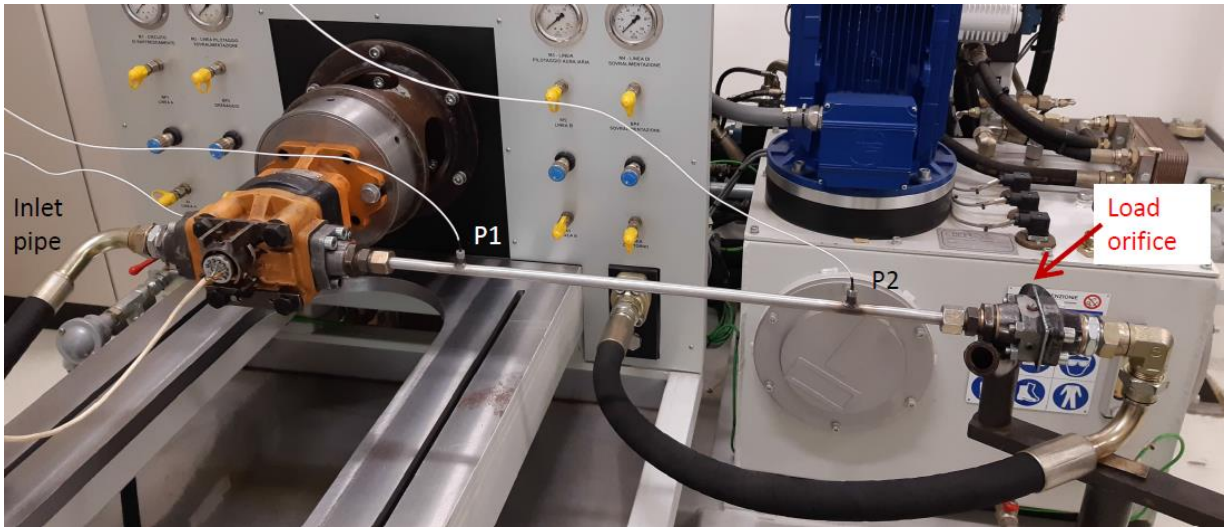

Figure 3: Photo of the pump mounted onto the test rig

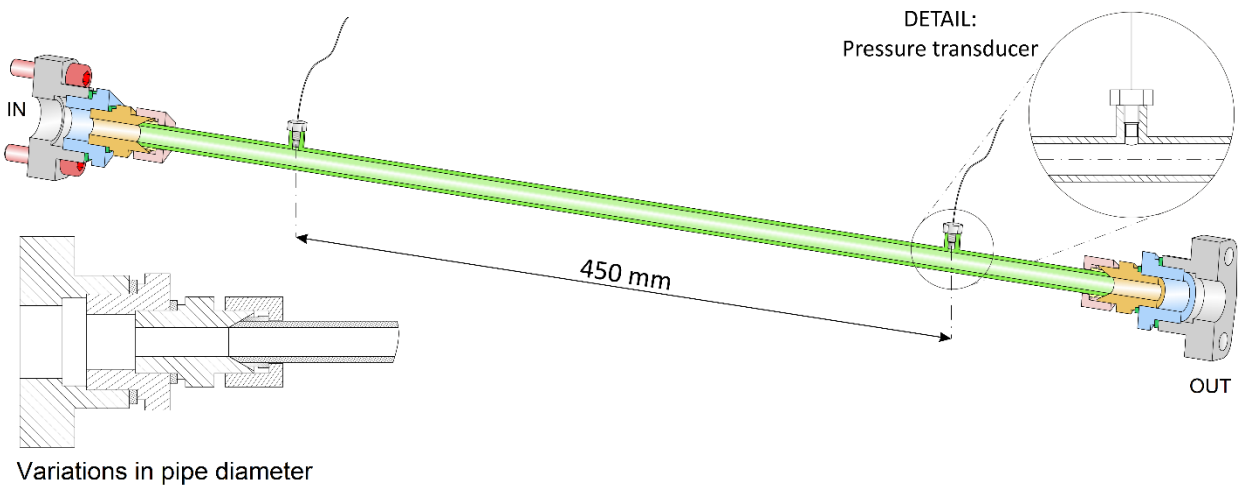

Figure 4: detailed view of the test-rig delivery line

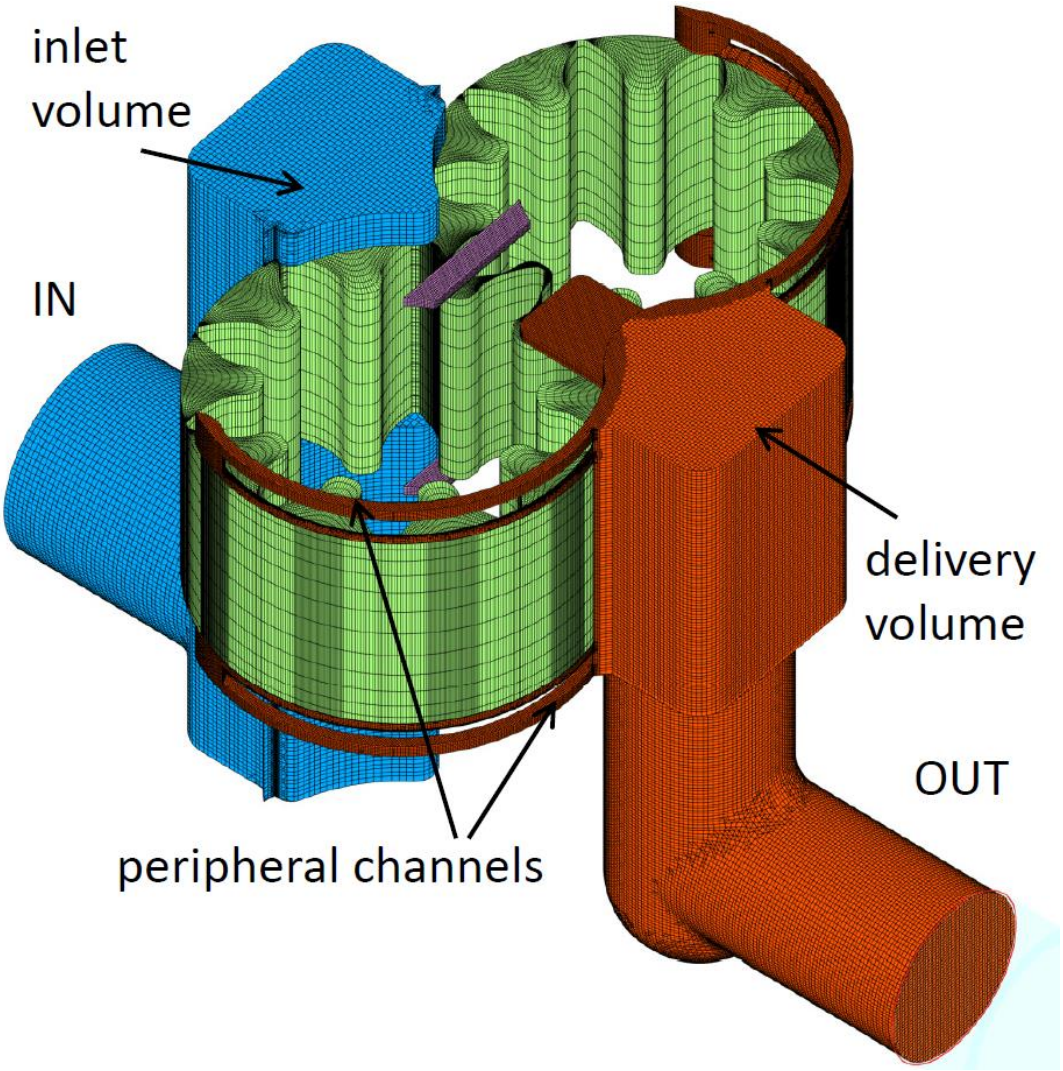

Figure 5: Model of the pump in Simerics MP+

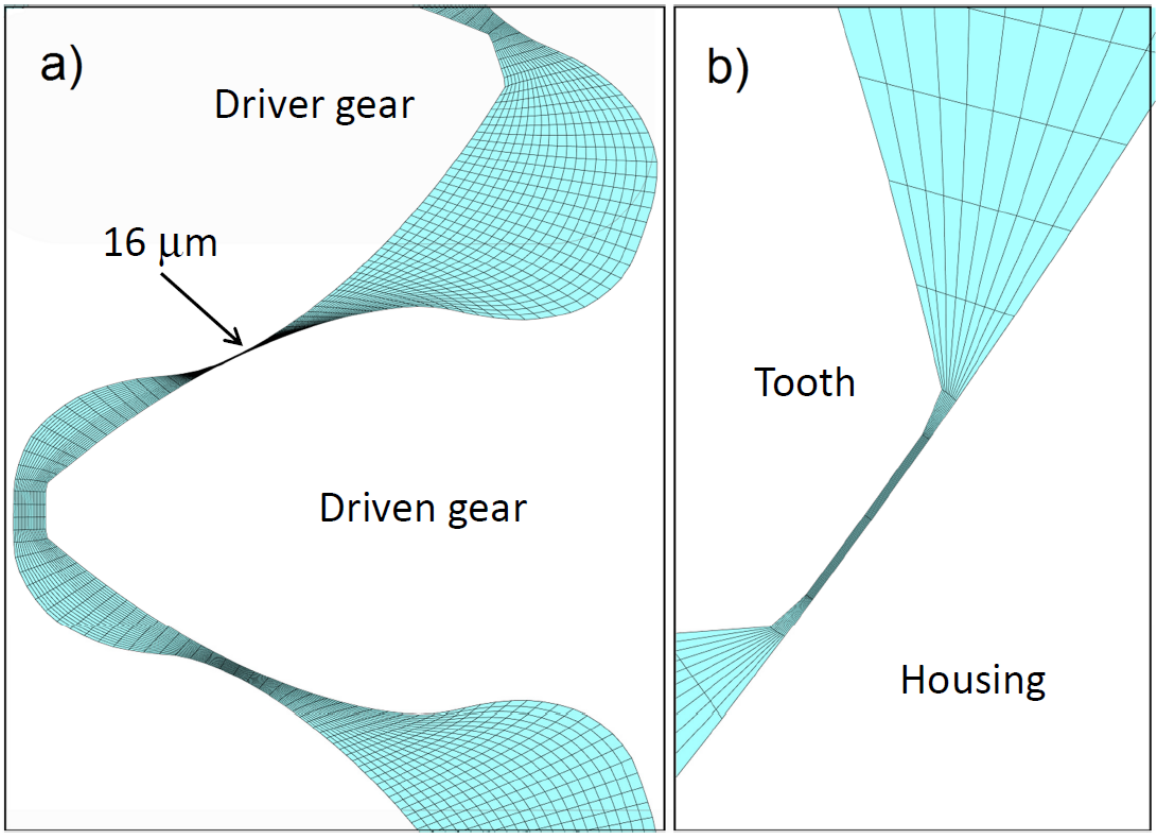

Figure 6: Details of the grid in the meshing region (a) and at the tooth tip (b)

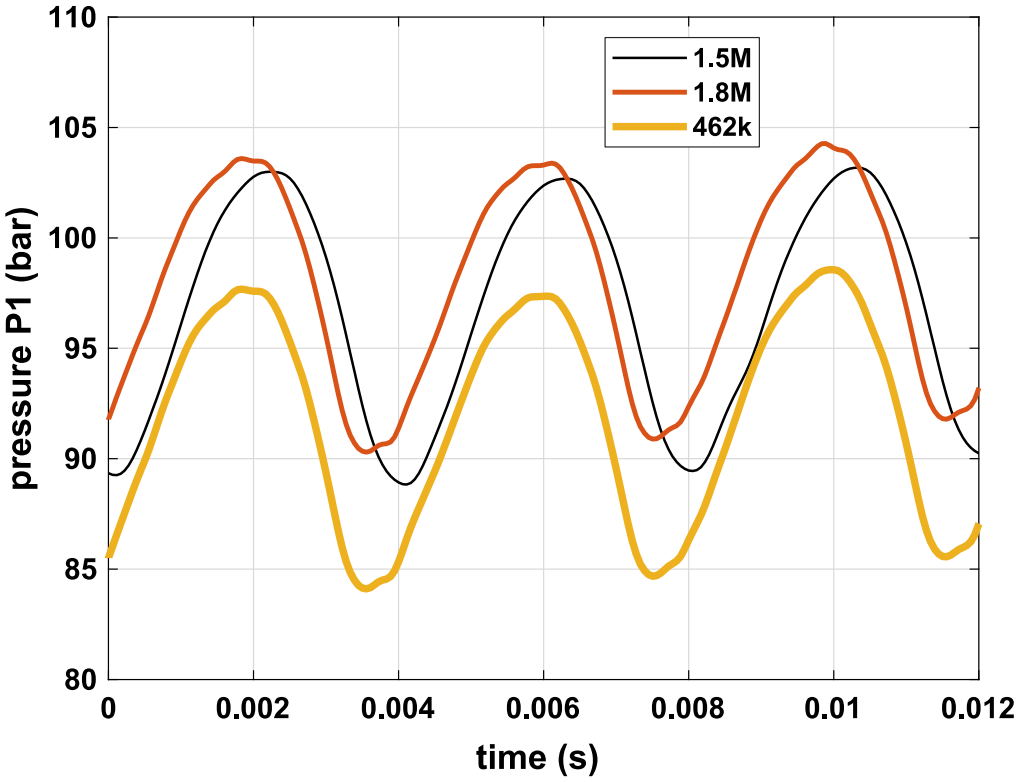

Figure 7: Influence of the number of cells on the instantaneous delivery pressure

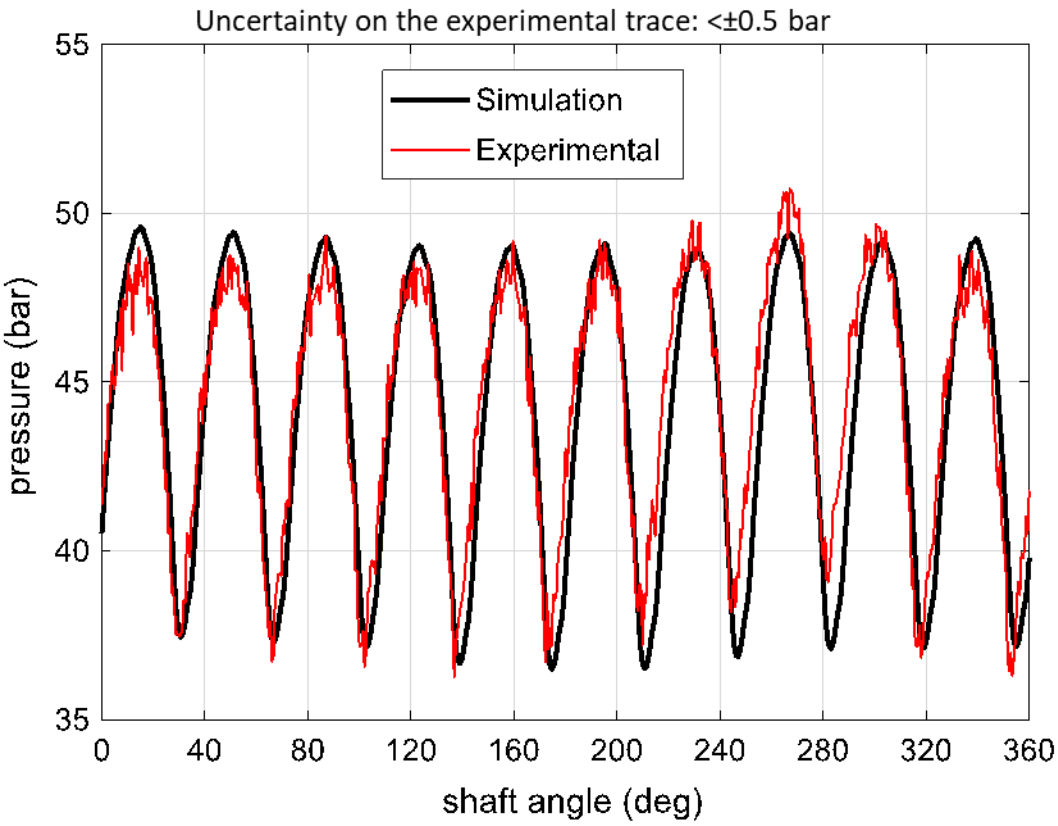

Figure 8: Pressure ripple at 1000 r/min and 45 *bar*

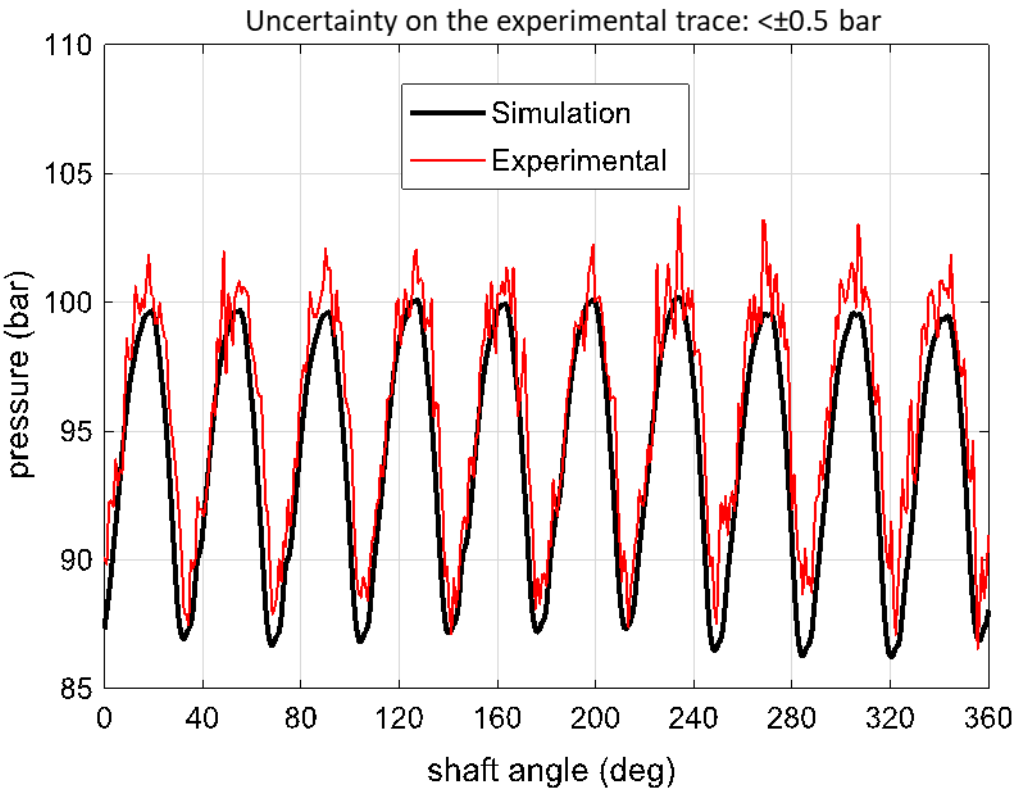

Figure 9: Pressure ripple at 1500 r/min and 95 bar

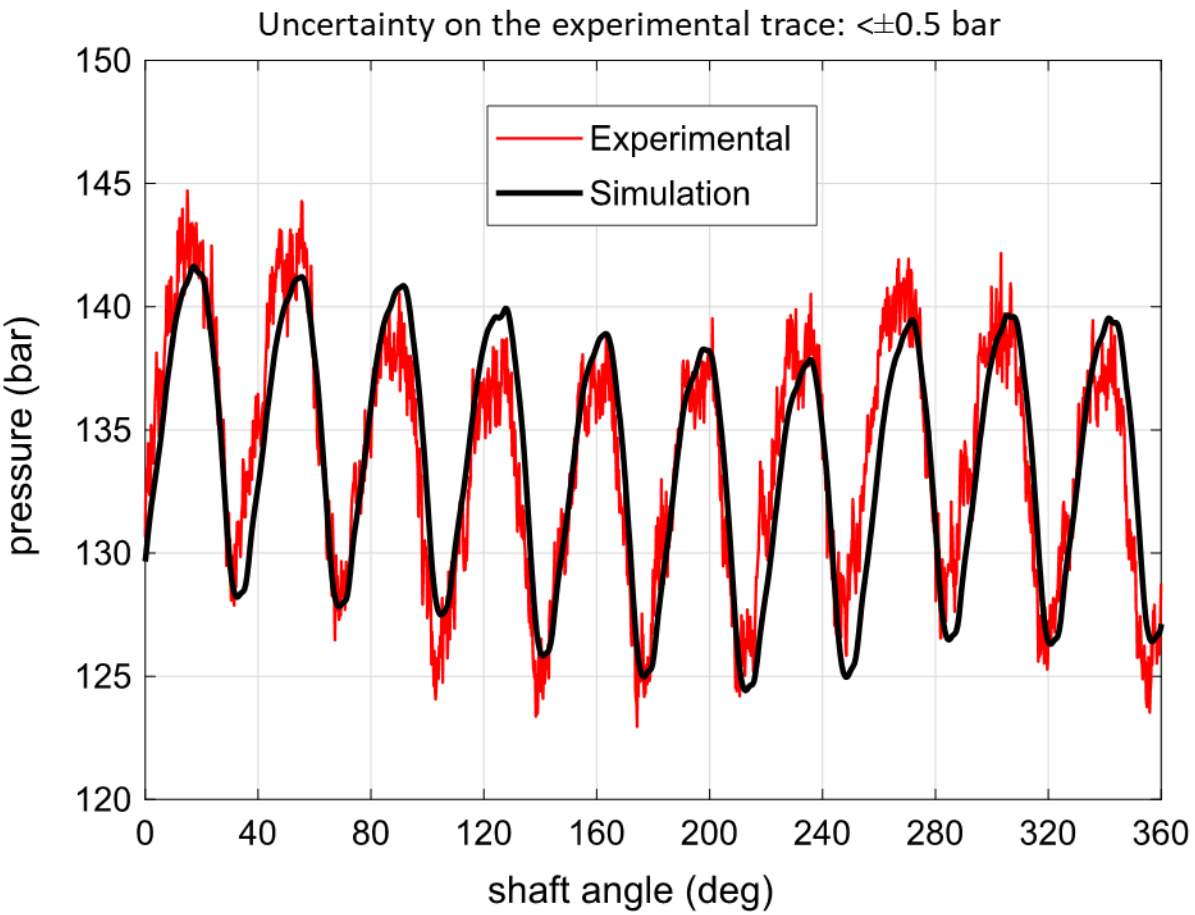

Figure 10: Pressure ripple at 1750 r/min and 133 bar

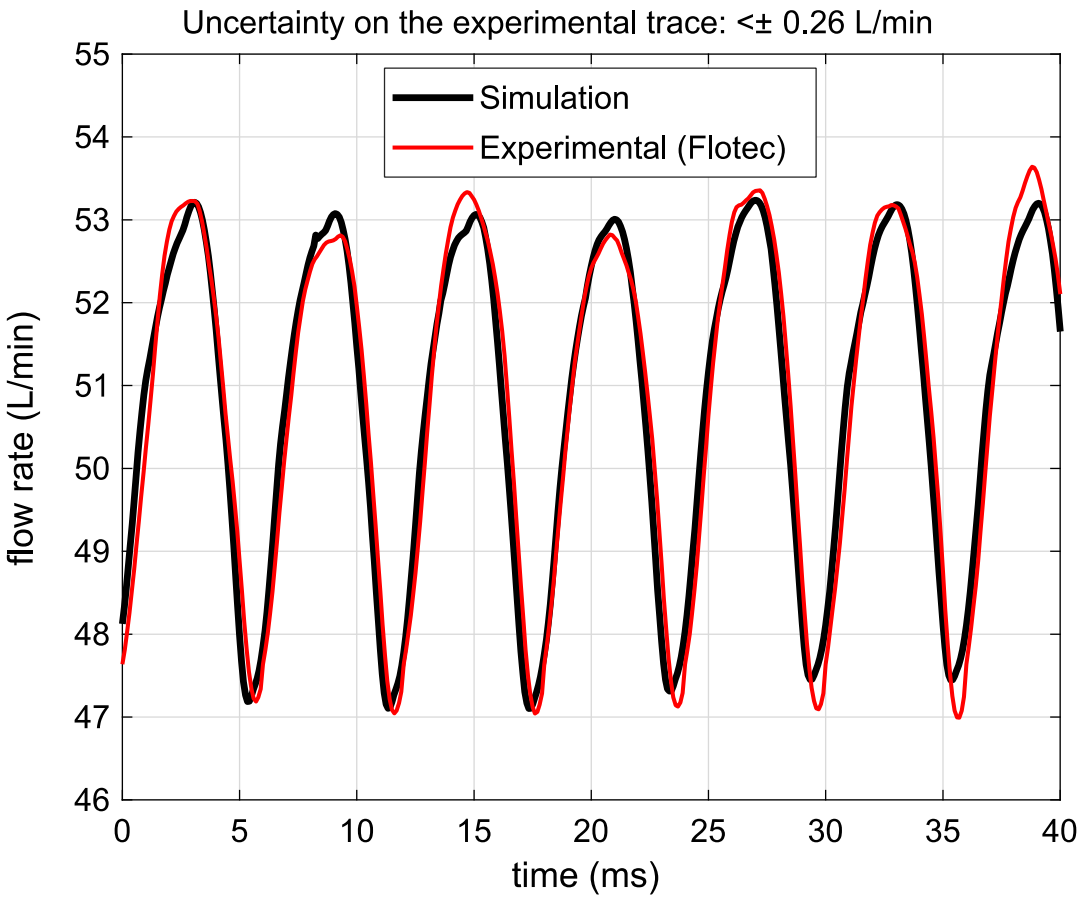

Figure 11: Comparison of the CFD model and the Flotec flow-rates (n=1000 rpm)

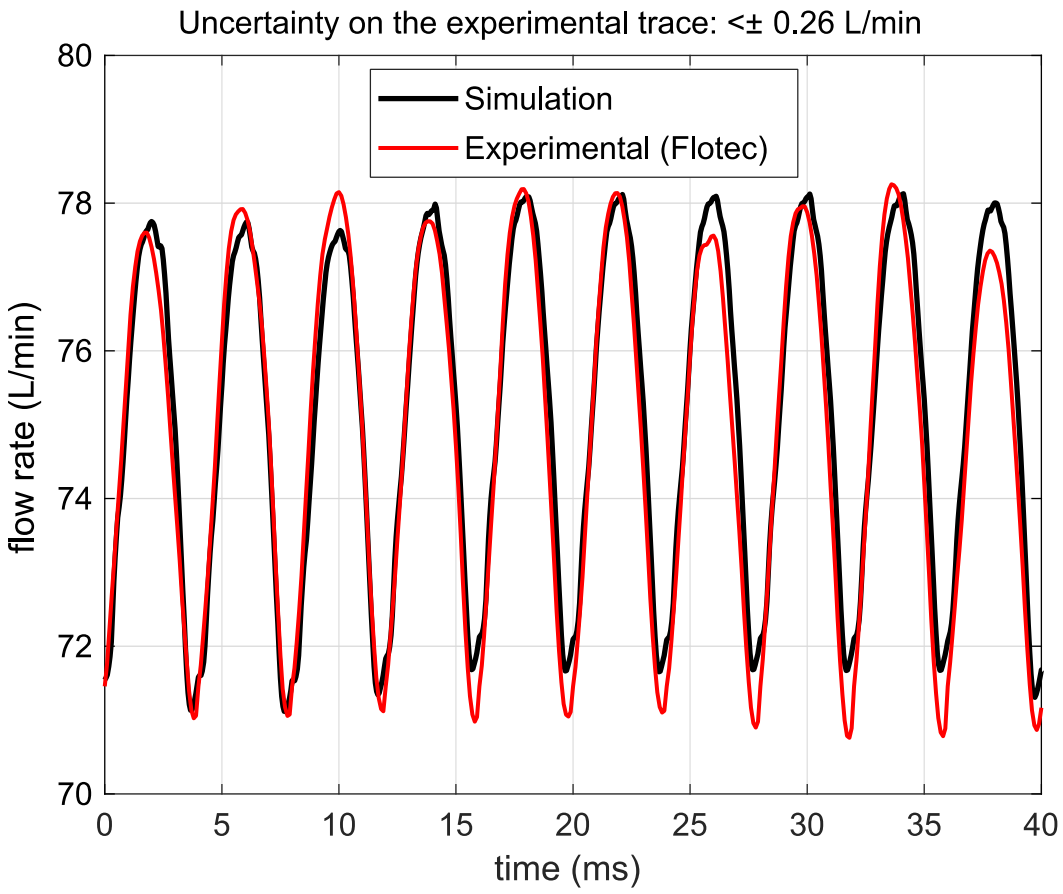

Figure 12: Comparison of the CFD model and the Flotec flow-rates (n=1500 rpm)

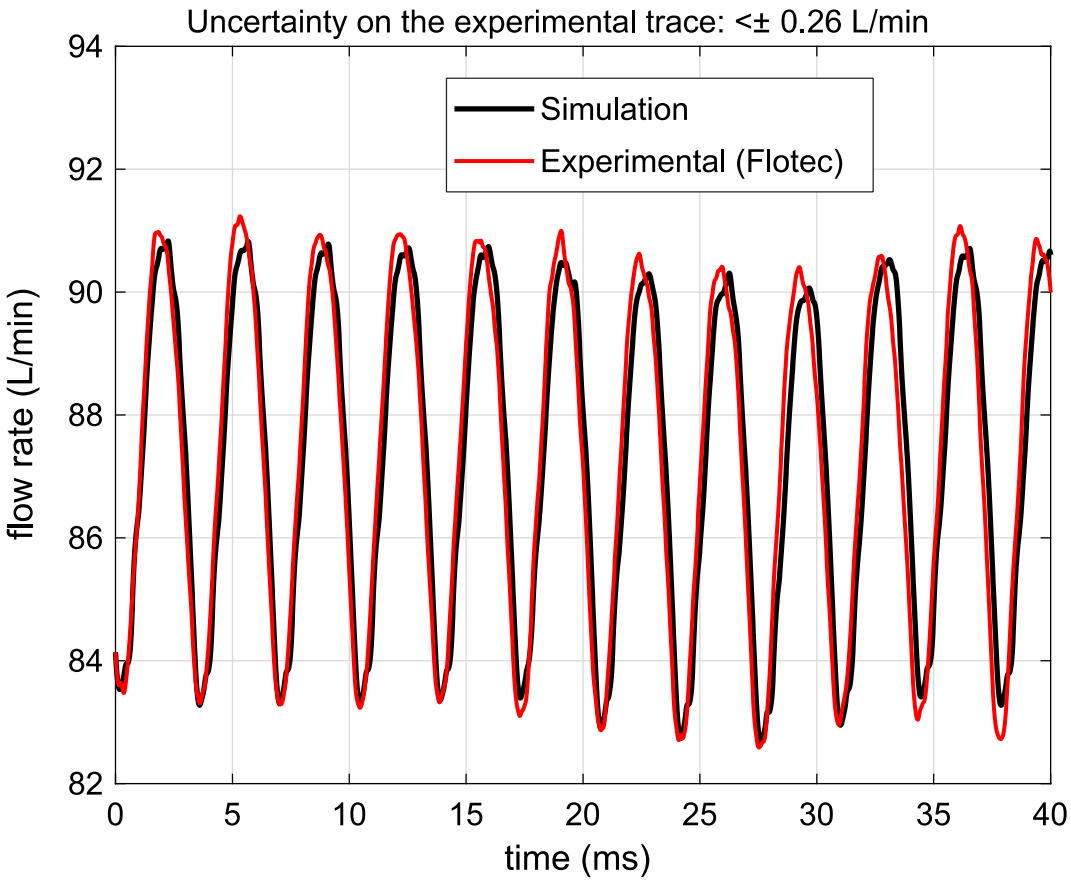

Figure 13: Comparison of the CFD model and the Flotec flow-rates (n=1750 rpm)

Table 1: Cell size for different fixed volumes

Volume	On the surfaces	Other cells (mm)
Delivery volume	0.5 mm	2 mm
Inlet volume	0.5 mm	3 mm
Port plate	0.26 mm	0.26 mm
Pipe	0.5 mm	1 mm